J. Fluid Mech. (2004), *vol.* 503, *pp.* 299–319.
DOI: 10.1017/S0022112004007918 Printed in the United Kingdom

Lock-release inertial gravity currents over a thick porous layer

By L. P. THOMAS[1], B. M. MARINO[1] AND P. F. LINDEN[2]

[1]Instituto de Física Arroyo Seco, Facultad de Ciencias Exactas, Universidad Nacional del Centro de la Pcia. de Buenos Aires, Pinto 399, B7000GHG Tandil, Argentina

[2]Department of Mechanical and Aerospace Engineering, University of California, San Diego, 9500 Gilman Drive, La Jolla, CA 92093-0411, USA

(Received 24 March 2003 and in revised form 20 October 2003)

This paper examines the motion of a dense fluid that develops as an inertial gravity current of decreasing mass above a horizontal porous bed, while flow described by Darcy's law occurs in the bed. Measurements of the mass and the front position of the current in a set of laboratory experiments performed by changing different parameters are presented. The results are explained by means of a global analytical model that suggests practical correlations combining the parameters. Thus, previous experimental, numerical and theoretical findings are extended to describe lock-release gravity currents above more realistic porous beds.

1. Introduction

Many environmental, geophysical and man-made flows in which a dense fluid is suddenly released on a horizontal boundary into a less dense surrounding medium, occur under the influence of gravity. This type of flow is often referred to as a gravity current and numerous examples in the environment and laboratory are reviewed by Simpson (1997). These flows are often modelled in the laboratory by releasing a finite volume of dense fluid, initially held behind a vertical barrier that separates it from the less dense ambient fluid. When the barrier is removed the differences in hydrostatic pressure on the two sides of the barrier drive a dense gravity current along the lower boundary. This is called a 'lock release' gravity current (Rottman & Linden 2001). The dense fluid is initially held in the finite lock and the barrier is referred to as the lock gate. Less dense fluid also flows in the opposite direction to the current into the lock.

The motion of such a gravity current on an impermeable horizontal bottom may be divided into three distinct phases. Initially the current accelerates and, if the Reynolds number is large enough, then travels at a constant speed. This constant–speed regime is associated with the fact that the volume flux from the lock is constant initially. The ambient fluid entering the lock eventually reaches the back wall of the lock and produces a disturbance that then propagates forwards in the same direction as the current. When the depth of the dense fluid within the lock is the same as the ambient fluid outside, the so-called 'full-depth lock release', this disturbance takes the form of a bore on top of the current. Rottman & Simpson (1983) showed that the bore travels faster than the current and eventually catches up with the front of the current after the latter has travelled about 10 times the original length of the lock. This time for the bore to catch the front is empirical, but well supported by experiment.

At this point the effects of the finite volume of dense fluid become important and the current begins to decelerate. From the results of experiments produced by instantaneous releases (Huppert & Simpson 1980; Rottman & Simpson 1983), theories (Fay 1969; Fannelop & Waldman 1972; Hoult 1972) and dimensional analysis (Rottman & Linden 2001) shows that, in a channel, the velocity decreases like $t^{-1/3}$. Eventually the current slows sufficiently and viscous effects become important. The onset of this third, viscous, phase depends on the initial conditions and if it is reached the velocity decreases as $t^{-4/5}$ (Didden & Maxworthy 1982; Huppert 1982; Marino *et al.* 1996).

Here we consider the propagation of the current over a horizontal porous bed. The bed is initially saturated with ambient fluid, and so the dense fluid in the current sinks into the bed, driven by the excess pressure at the top of the bed. It is expected that the loss of mass through the porous bed reduces the driving force for the current and thereby affects its velocity and depth. Gravity currents propagating over porous beds occur frequently in varied natural and man-made situations. Natural events include the currents of brackish water generated by tidal motions over the permeable bottom of estuaries, and internal waves impinging on continental shelves. Man-made situations include the release of sewage liquids on nearby coasts and the accidental escape of toxic liquids surrounded by gravel beds.

As an approximation to this problem Thomas, Marino & Linden (1998) studied the sudden release of fixed volumes of salt water over a permeable base consisting of two overlapping wire meshes. By changing the amount of overlap they were able to alter the permeability of the base. They focused on the case where the holes were small, so that the flow through the base was viscously controlled. They found, as had some preliminary experiments by Lionet & Quoit summarized in Simpson (1997), that the gravity current only travelled a finite distance before it stopped. This is in contrast to gravity currents on impermeable bases, which propagate continuously although, of course, with decreasing velocity. Thomas *et al.* (1998) found that the maximum distance the current travelled from the lock decreased with increasing density difference, suggesting that the loss of fluid through the base, which is driven by this density difference, plays a crucial role in the dynamics.

Moodie & Pascal (1999*a*) obtained numerical results on driven gravity flows over slightly sloping porous surfaces formed by the sudden release of a fixed volume of fluid. Their results for horizontal beds are in accordance with the experimental observations reported by Simpson (1997) for fixed values of porosity. Moodie & Pascal (1999*b*) also presented results concerning a two-layer shallow-water formulation for axisymmetric gravity currents overlaying a sloping porous bottom.

Ungarish & Huppert (2000) solved numerically the one-layer shallow-water equations for high-Reynolds-number gravity currents propagating over a horizontal porous boundary in both a rectangular and an axisymmetric geometry. One result of this paper was to show the effects of the impermeable bottom of the lock behind the lock gate on the initial phases of the motion of the current in the experiments of Thomas *et al.* (1998). An integral model that assumes the current has a constant height and a uniform density was also developed to provide estimates of the distance of propagation and average thickness as explicit functions of time.

Marino & Thomas (2002) studied the gravity currents travelling over a permeable surface in the case in which the flow through the porous base is limited by inertial effects, that is, when Darcy's law is not valid. The results provided by an analytical model, and corroborated by experiments, suggest that the mass of the current also

decays exponentially in this case, but with a decay constant that is different from the viscous case found by Thomas *et al.* (1998).

In all these papers the flow of dense fluid inside the porous bed is ignored. However, this flow is taken into account by Acton, Huppert & Worster (2001), who studied the evolution of a viscous gravity current (low Reynolds number) over a deep and (initially) unsaturated porous substrate. More recently, S. Khan & H. E. Huppert (2003, private communication) analysed the behaviour of a gravity current which propagates over and drains into a deep dry porous substrate where surface tension effects are relevant. On the basis of both shallow water and integral models of the current, it is found that the decay of the current volume above the porous bed is more closely approximated by a linear relationship. In this case the boundary condition of the flow through the porous medium is different from that considered here, and the partial analogy with the theoretical treatment developed in the present work will be examined in § 2.

Our previous experimental results (Thomas *et al.* 1998; Marino & Thomas 2002) were obtained by studying the behaviour of dense currents running over and through permeable surfaces such as grids. The flow through grids is only an approximation to flow in a porous medium. Although these studies have provided useful insights, in many practical circumstances the flow within a porous bed will change as the dense fluid enters it.

In this paper the behaviour of plane inertial gravity currents running over more realistic permeable layers of non-negligible thickness is investigated. Laboratory experiments were carried out in which fixed volumes of salt water were released from behind a lock with an impermeable bottom into a large rectangular cross-section channel containing fresh water. The current flows over a thick permeable layer, which is initially saturated with fresh water. As the salt water penetrates the bed, it drives the fresh water downwards in the bed, and out through the bottom. Measurements are presented of the gravity current and related to the loss of salt water from the current.

In § 2 we calculate the flow in the bed driven by a layer of salt water on top and its influence on the gravity current over the bed. This calculation is used to relate the present experiments to our earlier ones over a grid. The experiments are described in § 3, and the results are given in § 4. A summary and conclusions are given in § 5.

2. Dynamics of the flows involved

2.1. *Dense fluid penetration into a porous bed*

In order to study the behaviour of the gravity current, it is necessary to determine the flow into the porous medium. Specifically, consider a porous bed initially filled with fresh water over which a saline gravity current flows (figure 1). The boundary between the bed and the overlying fluid is at $z = 0$. If the gravity current travels significantly faster across the bed than the salt water intrudes into the porous medium, the dense fluid extends over an horizontal length much greater than the vertical depth through which the salt water has percolated into the porous medium. In such a case, the flow in the porous medium can be treated as one-dimensional (see figure 2), with the gravity current represented as a layer of fluid of constant depth h and density ρ_c.

We assume that the bed is initially saturated with fresh water and that as the salt water in the gravity current sinks into the bed, the fresh water beneath it flows downwards. Since the flow involves dense fluid over lighter fluid, the flow is

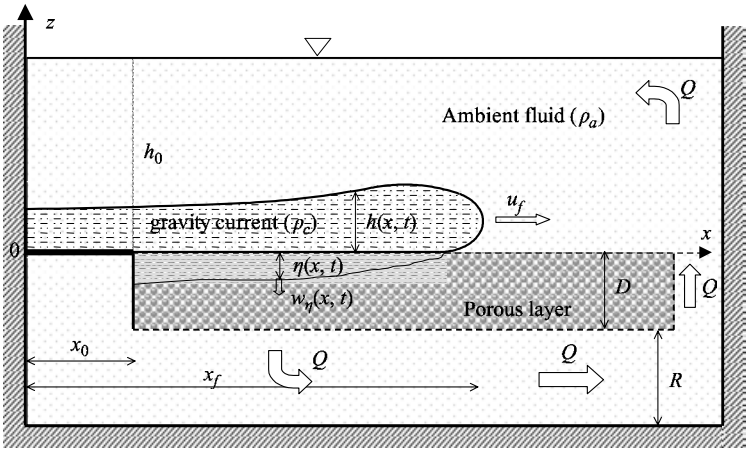

FIGURE 1. Schematic view of a gravity current above a permeable bed of thickness D. The lock gate is positioned at $x = x_0$, and the dense fluid initially occupies the full depth h_0 inside the lock. The percolation through the porous medium generates a horizontal flow Q in the free space under the porous layer without affecting the gravity current motion.

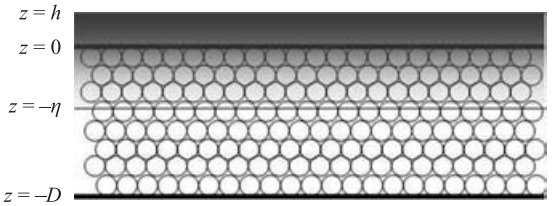

FIGURE 2. A schematic of the flow of dense fluid into the porous bed. The depth of the dense fluid above the bed is h and it has penetrated into the bed uniformly to a depth η.

statically unstable but, for the purposes of this discussion the possibility of convective instabilities is ignored.

The vertical Darcy velocity w within the bed is then given by Darcy's equation (Darcy 1856; Bear 1972)

$$w = -\frac{k}{\mu}\left(\frac{\partial p}{\partial z} + g\rho\right), \tag{2.1}$$

where k is the permeability, μ is the dynamic viscosity of the fluid, ρ is the density and g is the gravitational acceleration.

The pressure gradient driving the fluid from the current into the bed is given by the difference in pressures $p(0)$ at the top of the bed and the pressure $p(-\eta)$ at the interface $z = -\eta$ between the salt and fresh water. The pressure at the top of the bed is

$$p(0) = \int_0^\infty g(\rho_c - \rho_a)\,\mathrm{d}z, \tag{2.2}$$

where ρ_a is the density of the fluid initially in the bed. Both the initial densities of the fluid in the gravity current and in the bed can, in principle, be represented by functions of the height z. However, we will focus on the case in which ρ_a is a constant. Suppose, also, that the current is Boussinesq so $\rho_c \approx \rho_a$, then (2.2) reduces to

$$p(0) = \rho_a \int_0^\infty g'(z)\,\mathrm{d}z \equiv \rho_a \langle g' h \rangle, \tag{2.3}$$

where $g' = g((\rho_c - \rho_a)/(\rho_a))$ is the reduced gravity. The quantity $\langle g'h \rangle$, defined in (2.3) is the total buoyancy in the current at any x location. Hence the pressure gradient in the region above the interface $z = -\eta$ is $(p(0) - p(-\eta))/\eta$. The vertical Darcy velocity w_S in the salt water at the interface is given by (2.1) as

$$w_S = -\frac{k}{\mu}\left(\frac{\rho_a \langle g'h \rangle - p(-\eta)}{\eta} + g\rho_c\right). \tag{2.4}$$

At the bottom of the bed $z = -D$ the pressure is $p(-D) = g\rho_a D$, and the vertical Darcy velocity w_F in the fresh water is

$$w_F = -\frac{k}{\mu}\left(\frac{p(-\eta) - g\rho_a D}{D - \eta} + g\rho_a\right). \tag{2.5}$$

It is assumed that ρ_c is independent of position within the porous medium. Continuity requires that $w_S = w_F$, and hence the interface velocity w_η is given by

$$w_\eta = -\frac{k}{\nu}\frac{\langle g'(h + \eta) \rangle}{D}, \tag{2.6}$$

where $\nu = \mu/\rho_a$ is the kinematic viscosity of the ambient fluid, and g' is assumed independent of depth. In addition, the velocity w_η is related to the advance of the interface in the porous layer by

$$w_\eta = -\phi\frac{\partial \eta}{\partial t}, \tag{2.7}$$

where ϕ is the porosity of the medium.

S. Khan & H. E. Huppert (2003, private communication) show that for an initially dry porous medium the one dimensional percolation (2.6) is replaced by

$$w_\eta = -\frac{gk}{\nu}\left(1 + \frac{h}{\eta}\right) - \frac{p_c k}{\mu\eta}, \tag{2.8}$$

where p_c is an effective capillary pressure jump (Bear 1972; S. Khan & H. E. Huppert 2003, private communication). Some consequences of this different interface condition are discussed below.

2.2. *Gravity current over a porous bed*

Equations (2.6) and (2.7), which are valid for any x coordinate, have to be joined to relationships associated with the flow of the gravity current over the porous medium. In general, this is a complicated coupled problem and analytical solutions are only possible when simplifying assumptions regarding the gravity current flow are made.

The excess mass $m(t)$ per unit width of dense fluid above the porous bed is

$$m(t) = \int_0^{x_f(t)} \int_0^\infty (\rho_c(x, z, t) - \rho_a)\,\mathrm{d}z\,\mathrm{d}x, \tag{2.9}$$

where x_f is the position of the front. As fluid from the current enters the porous bed, mass conservation implies that

$$\frac{\mathrm{d}m}{\mathrm{d}t} = -\int_{x_0}^{x_f} (\rho_c(x, 0, t) - \rho_a) w_\eta\,\mathrm{d}x. \tag{2.10}$$

This mass conservation relationship can be employed to obtain an average value of w_η if $\mathrm{d}m/\mathrm{d}t$ is known. Provided the current does not mix with ambient fluid, (2.10)

may be written as

$$\frac{\mathrm{d}m}{\mathrm{d}t} = -(\rho_c - \rho_a)\ \overline{w_\eta}(t)\ (x_f(t) - x_0)\ , \tag{2.11}$$

where the overbar indicates the average along the permeable surface $x_0 \leqslant x \leqslant x_f$ covered by the current. Thus, (2.11) becomes

$$\overline{w_\eta}(t) = -\frac{\mathrm{d}m(t)/\mathrm{d}t}{(x_f(t) - x_0)(\rho_c - \rho_a)}, \tag{2.12}$$

which provides an estimate of the average vertical flow rate of the dense fluid per unit area through the porous medium, $\overline{w}_\eta$ – see § 4.

We now introduce the time scale τ_D

$$\tau_D = \frac{\nu D}{k g_0'}, \tag{2.13}$$

based on the reduced gravity g_0' of the initial release, first introduced by Thomas *et al.* (1998). For comparison, we recall that Marino & Thomas (2002) found a time scale

$$\tau = \frac{const}{\phi}\frac{a_0^{1/4}}{g_0^{1/2}},$$

instead (2.13), in the case of a porous layer of negligible thickness.

In addition, we define a mass scale $m_0 = (\rho_c - \rho_a)x_0 h_0 = \rho_a g_0' a_0$. Using these scales, the dimensionless mass $M = m/m_0$ and dimensionless time $T = t/\tau_D$, with $M(0) = 1$, are introduced. Also the horizontal and vertical lengths are non-dimensionalized by x_0 and h_0, respectively, and the reduced gravity by the initial value g_0'. Dimensionless variables are denoted by capital letters. Thus (2.10) can be expressed in the dimensionless form

$$\frac{\mathrm{d}M}{\mathrm{d}T} = -[M + M_\eta - M_1], \tag{2.14}$$

where

$$M = \int_0^{X_f} \langle G'H \rangle \, \mathrm{d}X \tag{2.15}$$

is the total mass remaining in the current obtained from (2.9),

$$M_\eta = \int_1^{X_f} \langle G'\eta \rangle \, \mathrm{d}X \tag{2.16}$$

is the mass in the porous medium, and

$$M_1 = \int_0^1 \langle G'H \rangle \, \mathrm{d}x \tag{2.17}$$

is the mass remaining in the lock.

Global mass conservation implies that

$$M + \phi\, M_\eta = 1 \tag{2.18}$$

and, therefore, (2.14) becomes

$$\frac{\mathrm{d}M}{\mathrm{d}T} = -\frac{1}{\phi}\left[1 - (1-\phi)\, M - \phi M_1\right]. \tag{2.19}$$

An analytical solution to this equation can be found when the mass remaining in the lock is small enough, i.e. $M_1 \ll M$. Integration of (2.19) from $T = 0$ leads to the

simple solution

$$M = \frac{1}{1-\phi}\left[1 - \phi \exp\left(\frac{1-\phi}{\phi} T\right)\right], \tag{2.20}$$

that does not depend on the height profile $h(x)$, the front evolution $x_f(t)$ and mixing, so that the result has significant generality. Equation (2.20) shows that the mass decays exponentially on a time scale defined by the porosity ϕ and τ_D, and that the time of extinction t_{END} of the current mass over the porous medium is finite and given by

$$t_{\mathrm{END}} = \frac{\phi}{(1-\phi)} \tau_D \ln\left(\frac{1}{\phi}\right). \tag{2.21}$$

Consider that a given initial condition introduces a small shift δT in the time origin of (2.20). The solution for $T > \delta T$ is

$$M_\delta = \frac{1}{1-\phi}\left[1 - \phi \exp\left(\frac{1-\phi}{\phi}(T - \delta T)\right)\right]. \tag{2.22}$$

The difference ΔM between this solution and that given by (2.20) is

$$\Delta M = M_\delta - M \simeq \exp\left(\frac{1-\phi}{\phi} T\right) \delta T. \tag{2.23}$$

Therefore, ΔM increases with time T; this behaviour is different from that found for currents over thin substrates (Thomas *et al.* 1998) or the similar solutions on impermeable boundaries (Rottman & Simpson 1983). This is probably because the flow through the porous medium depends not only on the mass in the current M, but also on the mass in the porous bed M_η as shown by (2.14).

The solution (2.20) makes sense for $x_f \gg x_0$, that is, in the later stages of the flow. However, (2.23) shows that (2.20) may contain a significant accumulated error when (2.19) is integrated from $T = 0$.

On the other hand, in the early stages of the flow the mass of fluid M_1 retained in the lock is not negligible. In such a case the motion of the front of the current is important, and the speed may be associated with a constant Froude number F by the relation

$$\frac{\mathrm{d}x_f}{\mathrm{d}t} = F \sqrt{\langle g' h \rangle}, \tag{2.24}$$

where the right side must be evaluated at the front of the current. The empirical formula introduced by Huppert & Simpson (1980),

$$F = \begin{cases} 1.19, & 0 < H < 0.075 \\ H^{-1/3}, & H > 0.075, \end{cases} \tag{2.25}$$

is used, although we found that $F = const$ gives also acceptable results in the determination of $M = M(T)$.

Using dimensionless variables (2.24) becomes

$$\frac{\mathrm{d}X_f}{\mathrm{d}T} = F\, \lambda \sqrt{\langle G' H \rangle}, \tag{2.26}$$

where

$$\lambda = \frac{\tau_D}{t_c} \tag{2.27}$$

is the ratio between the characteristic time τ_D of the vertical flow through the porous medium given by (2.13), and

$$t_c = \frac{x_0}{\sqrt{g_0' h_0}}. \tag{2.28}$$

The characteristic time t_c is proportional to the time it takes for the gravity current to travel the length of the lock, and so measures the time scale for the finite lock volume to become important. The time scales are ratios between a length scale and the corresponding velocity, so that

$$\lambda = \frac{\tau_D}{t_c} = \frac{h_0}{x_0}\frac{\sqrt{g_0' h_0}}{\nu D/k} \tag{2.29}$$

may also be thought of as the ratio of the horizontal and vertical characteristic velocities times the initial geometrical aspect ratio.

Equations (2.19) and (2.26) constitute a pair of coupled differential equations whose solutions depend on the horizontal variations in the height $h(x)$ and reduced gravity $g'(x)$. The simplest case to consider is an integral model in which the current is represented as a rectangle of constant depth $h(x) = h$ and uniform density $g'(x) = g'$. As we will see in §4.1 the observed currents do have fairly uniform values of g' along their length, but the depth increases significantly from the rear to the front. We discuss the relation of the observed current to this model in §4. In the case of this simplified integral model, from (2.15) and (2.17) it follows that

$$M = \langle G'H \rangle X_f \tag{2.30}$$

and

$$M_1 = \langle G'H \rangle . \tag{2.31}$$

Then (2.19) and (2.26) become

$$\frac{\mathrm{d}M}{\mathrm{d}T} = -\frac{1}{\phi}\left[1 - (1-\phi)M - \phi\frac{M}{X_f}\right] \tag{2.32}$$

and

$$\frac{\mathrm{d}X_f}{\mathrm{d}T} = F\lambda\sqrt{\frac{M}{X_f}}. \tag{2.33}$$

An analytical solution can also be obtained for $M_1 \ll M$, but the general case is solved by using any simple integrator of ordinary differential equations. The total mass in the porous medium M_η is calculated from this solution and (2.18).

The profile $\eta(x,t)$ of the interface between dense and ambient fluids inside the porous bed may also be determined numerically. From (2.6) and (2.7), it follows that

$$\phi\frac{\mathrm{d}\eta}{\mathrm{d}t} = \frac{k}{\nu}\frac{\langle g'(h+\eta)\rangle}{D} \tag{2.34}$$

that becomes in the dimensionless relationship

$$\phi\frac{\mathrm{d}N}{\mathrm{d}T} = \langle G'(H+N)\rangle, \tag{2.35}$$

where $N = \eta/h_0$. Using (2.30) and assuming no mixing inside the porous medium, we obtain

$$\phi\frac{\mathrm{d}N}{\mathrm{d}T} = N + \frac{M}{X_f}. \tag{2.36}$$

The numerical solution of (2.32)–(2.33) is used to calculate the right hand side of (2.36), and the interface position N for a fixed X is obtained by time-integrating the interface velocity $\mathrm{d}N/\mathrm{d}T$ starting from the time at which the front of the current passes through X.

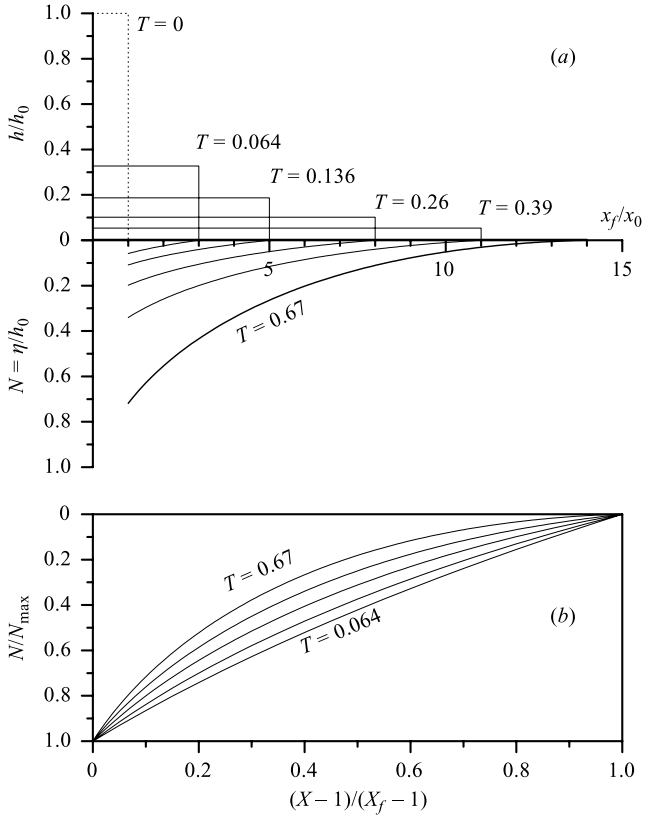

FIGURE 3. (*a*) Typical profiles of the current over and inside the porous medium obtained for $\lambda = 70$ and $\phi = 0.375$. (*b*) Shape of interface inside the porous medium shown in (*a*).

Figure 3(*a*) shows the profiles obtained at different times for typical parameter values. The corresponding profiles of the current over the porous layer are also included to complete the picture. Figure 3(*b*) illustrates the shapes of the interface profiles in the porous layer. These profiles evolve from an almost linear initial shape to a concave shape at later times. The penetration into the porous bed is greatest near the lock, since the current is deeper there and the bed is covered by the gravity current for the longest time.

The profile shapes and their time evolution shown in figure 3(*b*) are different from those profiles obtained for the flow into a deep dry porous medium. In the latter case the boundary condition at the interface may retard the rate of drainage near the origin at later times giving, as a consequence, a convex shape (see figure 4 of Khan & Huppert 2003).

3. The experiments

Gravity currents were generated in a long rectangular tank with transparent Perspex sidewalls by means of a lock-exchange system. Dense salt solution was initially held in a confined region behind a vertical barrier – the lock gate. The current was initiated by carefully lifting the gate. The tank, 3 m long, 0.2 m wide and 0.6 m deep, is approximately 50% longer than that used by Thomas *et al.* (1998), allowing for a longer evolution of the current along the tank.

A porous layer was composed of glass spheres with an average diameter of 0.286 cm. The porosity of the matrix was measured by pouring the dry spheres into a calibrated cylinder of known volume, and then adding water to the top of the packed spheres. The porosity ϕ was determined by weighing the cylinder before and after the water was added. We found that $\phi = 0.375$.

The glass spheres were contained in a specially constructed container consisting of thin Perspex sidewalls. The container was placed above the bottom of the tank and abutted the end of the lock. The lock had an impermeable base. When the gate was lifted the current flowed along the top of the porous layer (see figure 1).

The bottom of the container holding the glass spheres was made of a highly permeable mesh and was located at a distance $R = 0.12$ m above the bottom of the tank. Initially the tank was filled with fresh water to a depth h_0 above the porous boundary. The porous bed was saturated with fresh water, which also initially occupied the space beneath the bed.

When the gate was raised, dense salt solution flowed out along the top of the porous bed. The excess pressure produced by the dense fluid on top of the bed, forced a flow inside the bed. Fresh water was driven out through the mesh base and flowed along the unobstructed channel beneath the bed. In order to limit the interaction between the flow Q of fresh water drained away from the bed, and the gravity current, a space was left between the porous medium and the endwall of the tank (see figure 1). We find that the most of the fresh water goes upwards through this unrestricted opening and the residual flow through the bed does not affect the dynamics of the gravity currents. After each run the porous bed was washed with fresh water and dried with warm air in order to avoid random bubbles beneath and inside the bed that can affect the reproducibility of the results.

The lock was formed by a vertical gate located at a distance x_0 from the rear wall. Two values of x_0, 0.10 m and approximately 0.20 m, were used. In both cases the tank length was longer than 10 lock lengths, so the transition from the constant velocity phase to the similarity phase (see § 1) is expected to occur if the currents were travelling over an impermeable base. Dense salt solution, density ρ_c, with a small amount of dye for visualization, was added behind the gate and was filled to the same depth as the fresh water, density $\rho_a < \rho_c$, in the tank, so that these were 'full-depth lock releases'. In every case the length of the lock x_0 was smaller than its depth h_0. Two depths D, 0.09 m and 0.12 m, of the porous bed were used. The driving force for the flow is described by the reduced gravity $g'_0 = g[(\rho_c - \rho_a)/\rho_a]$. The maximum value of g'_0 was 73 cm s^{-2}, and the currents were Boussinesq. Table 1 lists the main parameters for the 33 experiments.

A panel of lights with a diffusing screen located behind the channel provided nearly uniform back-lighting. A video camera was placed at a fixed position 6 m away from the tank. The images captured by the video camera were stored in a PC and digitally processed. Measurements of the light intensity are obtained for each pixel. These are related to the concentration of the dye along each light path and so provide the width averaged dye concentration. The dye concentration is related to the width averaged salt concentration, since the dye acts as a passive tracer. Thus the intensity measurements give the full two-dimensional density distribution $\rho(x, z, t) - \rho_a$ on each video frame (Thomas *et al.* 1998), and the relative mass m per unit width (2.9) is obtained by integration. Because of the opacity of the glass spheres it was only possible to obtain density measurements above the porous layer.

The presence of dissolved salt increases the refraction index of water. Variations in the refraction index may modify the light intensity captured by the camera, which

Run	x_0 (cm)	h_0 (cm)	g'_0 (cm s^{-2})	D (cm)	t_c (s)	τ_D (s)	τ_{expt} (s)	λ
1	10.0	25.6	10.9	12.0	0.599	202	189	337
2	10.0	25.6	20.1	12.0	0.441	109	108	248
3	10.0	25.6	30.1	12.0	0.360	73.1	73.0	203
4	10.0	25.6	39.2	12.0	0.316	56.1	62.3	178
5	10.0	25.6	49.0	12.0	0.282	44.9	44.6	159
6	10.0	25.6	65.1	12.0	0.245	33.8	32.9	138
7	19.6	25.6	4.2	12.0	1.89	524	510.0	277
8	19.6	25.6	5.8	12.0	1.61	379	402.0	236
9	19.5	25.6	11.2	12.0	1.15	196	189.0	171
10	19.6	25.6	13.6	12.0	1.05	162	178.0	154
11	19.6	25.6	18.8	12.0	0.893	117	119.0	131
12	19.7	25.6	24.5	12.0	0.787	89.8	98.4	114
13	19.4	25.6	27.4	12.0	0.732	80.3	80.2	110
14	19.6	25.6	33.4	12.0	0.670	65.9	64.5	98.3
15	19.4	25.6	38.3	12.0	0.620	57.4	55.0	92.7
16	19.6	25.6	44.1	12.0	0.583	49.9	51.6	85.5
17	19.4	25.6	46.9	12.0	0.560	46.9	44.8	83.8
18	19.6	25.6	55.5	12.0	0.520	39.6	41.3	76.2
19	19.6	25.6	62.5	12.0	0.490	35.2	35.2	71.8
20	19.5	25.6	73.4	12.0	0.450	30.0	31.0	66.6
21	19.9	20.0	2.8	9.0	2.66	589	587.0	222
22	19.6	20.0	9.8	9.0	1.40	168	165.0	120
23	19.7	20.0	19.6	9.0	0.995	84.2	88.3	84.6
24	20.0	20.0	36.5	9.0	0.740	45.2	45.2	61.1
25	19.7	20.0	63.0	9.0	0.555	26.2	28.1	47.2
26	10.0	25.0	1.9	9.0	1.45	868	790.0	599
27	10.0	25.0	2.8	9.0	1.20	589	555.0	493
28	10.0	25.0	6.0	9.0	0.816	275	273.0	337
29	10.0	25.0	11.9	9.0	0.580	139	133.0	239
30	10.0	25.0	21.6	9.0	0.430	76.4	77.0	178
31	10.0	25.0	41.6	9.0	0.310	39.7	39.7	128
32	10.0	25.0	51.0	9.0	0.280	32.4	31.8	116
33	10.0	15.0	20.9	9.0	0.565	78.9	76.5	140

TABLE 1. Main parameters of the experiments.

affects the density measurements. There are several standard ways to overcome this problem (Dalziel 1995; Merzkirch 1987). We performed a correction that we tested with an additional set of experiments carried out over a transparent solid base and without adding dye to the current or the the ambient fluid. As expected, the amount of correction increased with the density of the current and inversely with its depth. After image processing the relative mass m per unit width was obtained with an error less than 2% (Dalziel 1995).

4. Results

4.1. *Qualitative observations*

Figure 4 shows the gravity current in Experiment 9. This experiment is typical of all the experiments we carried out. The images are in false colour, which is related to the density in the current. These images show a number of features, some of which are observed in currents over an impermeable base, while others are a result of the penetration into the bed. In the initial stages the flow from the lock

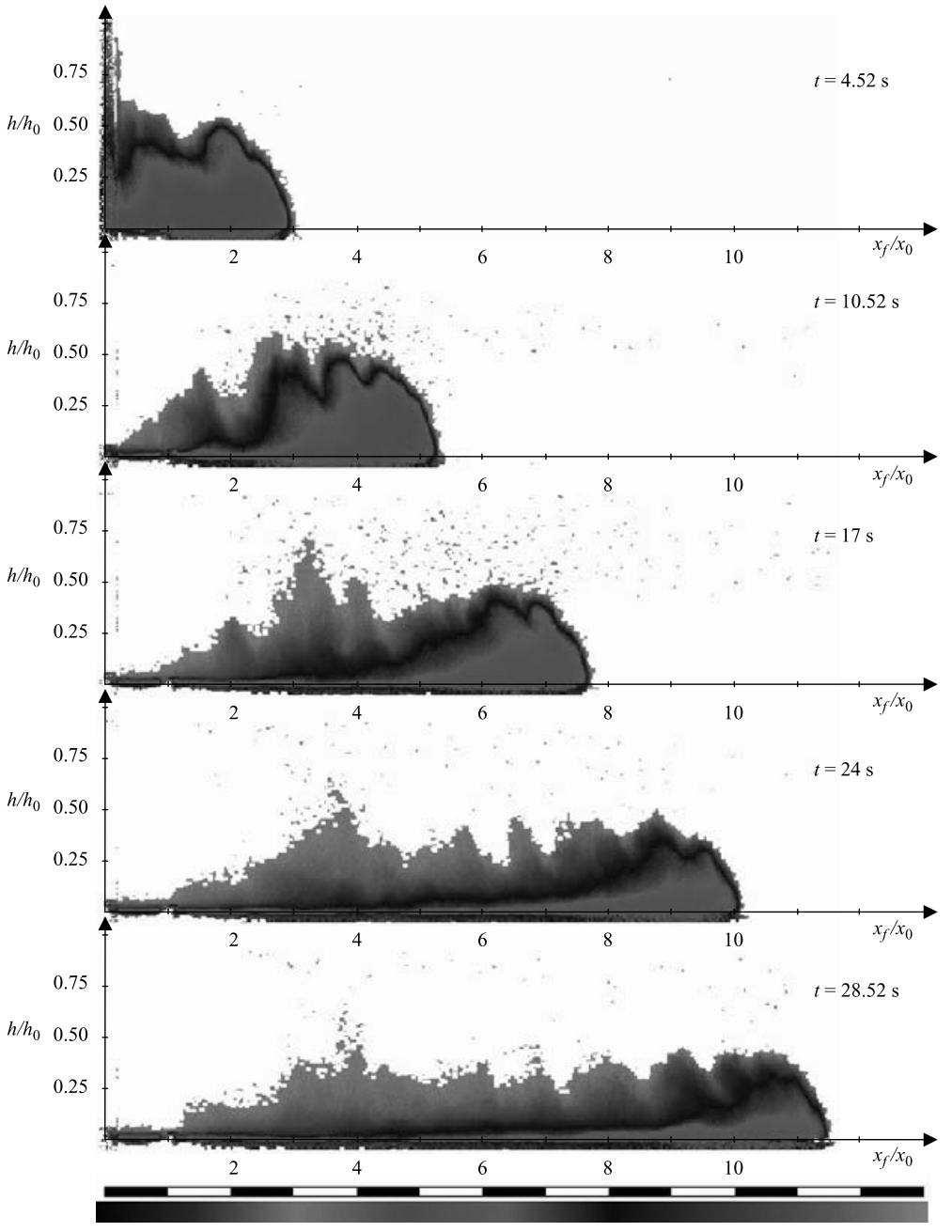

FIGURE 4. Grey-scale representation of the motion of a gravity current over a porous bed. The distance in lock-lengths and the intensity scale are shown at the bottom of the figure.

is essentially the same as over a solid base – see, for example, similar images in Hacker, Linden & Dalziel (1996). Fluid moves horizontally at the base of the lock and billows form on the top of the current. The density in the bulk of the current remains unchanged during this collapse. The front of the current is marked by a sharp density change, and a head, deeper than the following current, forms.

As the current propagates, there are three main changes from the solid bed case. The depth of the dense fluid behind the front decreases with time, the density in the head also decreases (as can be seen by the change in colour) and there is evidence of some disruption to the interface at the top of the current. These changes are a result of the penetration of dense fluid into the porous bed which, unfortunately, is not visible in these images due to the opaqueness of the bed. The decrease in current depth at any given horizontal location is almost all due to this penetration, since over a solid base the depth remains nearly constant during the constant velocity phase. We observed fresh water driven out through the base of the bed by this penetration, but it was not possible to measure this flow accurately.

It seems, however, and in contrast to the model in § 2, that some of the fresh water within the bed also rises upwards through the bed and the current. This fluid is driven by a Rayleigh–Taylor instability produced by the salt water in the current on top of the fresh water. This forms convective plumes that disrupt the top of the current, and carry with them some of the salt water. The mixing associated with this process also dilutes the salt water within the current and causes the density within the current to decrease with time.

While this convectively-driven flow changes the look of the current it does not appear to have a first order effect on the dynamics. Both the horizontal speed of the current and the penetration of the salt water into the bed, depend on $\langle g'h \rangle$, the total buoyancy in the current. If, as is appropriate, we include all fluid with density larger than the ambient fresh water as being in the current, then this total buoyancy is not altered by the convective action above the bed. The additional mixing reduces the density but increases the volume, keeping $\langle g'h \rangle$ constant.

The convectively-driven flow above the current does induce additional turbulence in the current, the effect of which may be to decelerate the current (Linden & Simpson 1986). Also, there is an enhanced penetration of salt water into the bed, driven by a corresponding convective flow in the porous medium. This would be the only penetration, for example, if the bed had an impermeable base which prevented any fluid from being displaced below it. We will show in § 4.2 that an adequate model of the current can be derived even when these effects are ignored and so we conclude that these convective effects are not of prime importance (see also § 5).

4.2. *Quantitative observations*

The mass of the current is of interest because it is related to the driving force of the current and can be directly obtained with the diagnostics described above. Figure 5(*a*) illustrates the evolution of the dimensionless mass $M(t) = m(t)/m_0$ of the current plotted against the time t measured from release for $D = 12\,\text{cm}$, $a_0 \approx 500\,\text{cm}^2$ and different values of g'_0. As the current propagates over the porous bed, the results show that the mass of the gravity current decreases at a rate that increases with g'_0. Figure 5(*b*) shows the data in figure 5(*a*) using the dimensionless time $T = t/\tau_D$, where τ_D is the characteristic time defined by (2.13). We see that, with this scaling, the experimental values of M for all the experiments collapse on to a single curve, within experimental accuracy.

There are three theoretical curves shown on this figure. The dashed line is the result of the integral model (2.20) for the case $x_0 = 0$ corresponding to a lock of zero length. This solution underestimates the mass in the current since it does not account for the mass remaining above the impermeable base in the lock, and does not result in a good approximation to the experimental behaviour. The solid curves on figure 5(*b*)

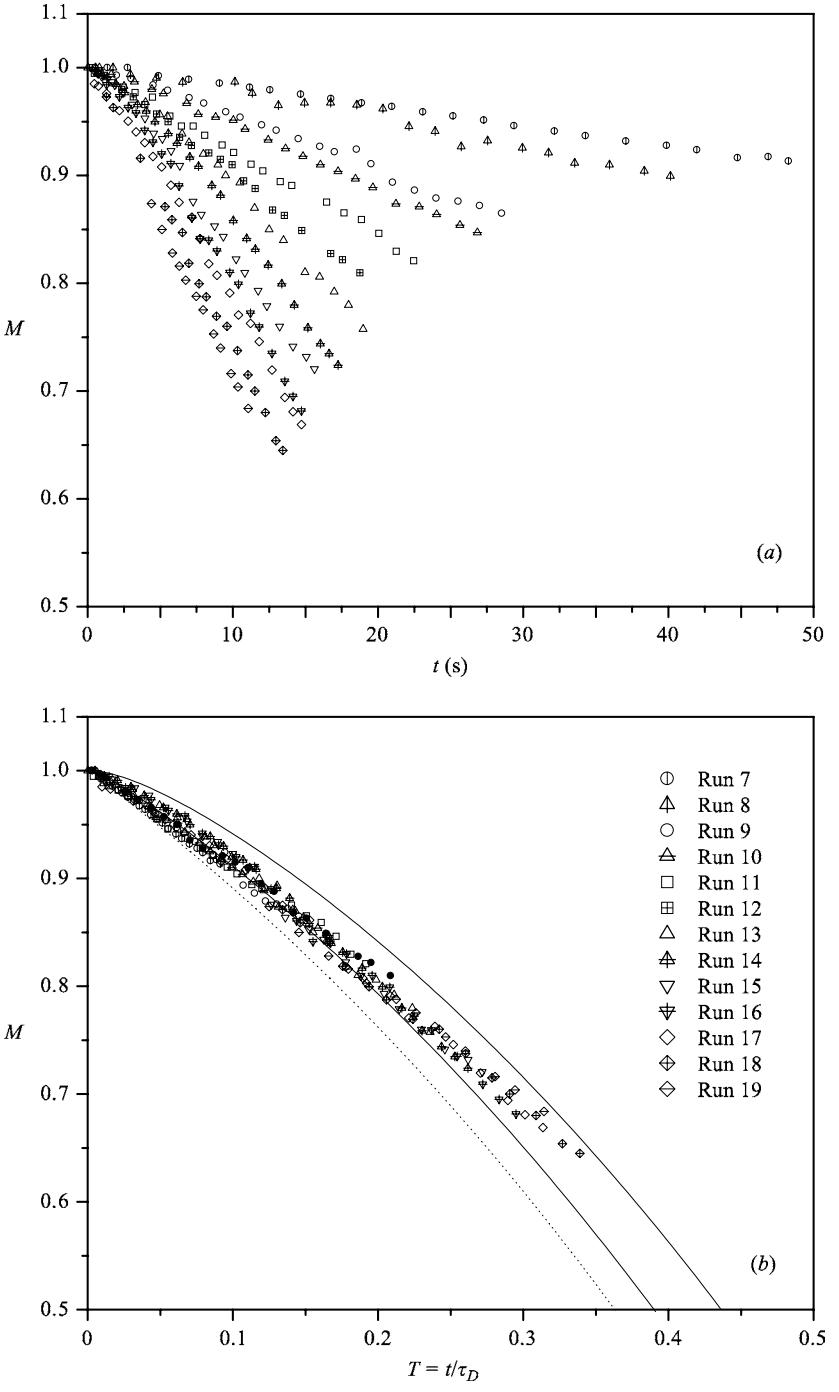

FIGURE 5. Dimensionless mass M remaining in the current for a porous bed of thickness $D = 12\,\text{cm}$, $a_0 \approx 500\,\text{cm}^2$ and different g'_o as a function of (a) time t measured from release and (b) dimensionless time using (2.13). The dashed line is given by (2.20), while the solid lines correspond to solutions of the integral model with the minimum (70) and maximum (280) values of λ of the experiments shown.

are the solutions corresponding to the integral model (2.32)–(2.33) associated with the highest and lowest values of λ in the present experiments.

Figure 6 shows the equivalent plots as in figure 5 for the case $D = 9\,\mathrm{cm}$ and several combinations of a_0 and g_0'. Again the data collapse with the time scaled on τ_D and the integral model gives a good representation of the data. The good agreement between the model developed in § 2 and the experimental results, occurs because the model includes the effects on $M(t)$ of the finite lock length, which may be taken into account by employing the parameter $\lambda = \tau_D/t_c \neq 0$. However, the effects on the flow are not the same that those indicated by Ungarish & Huppert (2000) as they did not consider the contribution of the weight of the fluid inside the porous medium.

Figure 7(*a*) illustrates the evolution of the location of the front of the current with time. Two sets of experiments are shown. The first set (runs 1–6, see table 1)) have a short lock $x_0 = 10\,\mathrm{cm}$, while the second set (runs 7–20, see table 1) have a longer lock $x_0 = 20\,\mathrm{cm}$. Since the tank is 3 m long the currents have the potential to travel further than 10 lock lengths, and so to change from the constant-velocity phase to the similarity phase. Figure 7(*b*) shows the dimensionless front position $(x_f(t) - x_0)/x_0$, plotted against the dimensionless time t/t_c for $D = 12\,\mathrm{cm}$ and two values of x_0.

Also shown on figure 7(*b*) are the constant-velocity and the similarity predictions for impermeable lower boundaries. The constant-velocity line is given by a Froude number $F_0 = u/(\sqrt{g_0' h_0}) = 0.46$, based on the initial depth in the lock. The similarity solution $x_f(t)/x_0 = 1.5(t/t_c)^{2/3}$ is plotted by a dashed line using the empirical coefficient obtained by Rottman & Simpson (1983), Huppert & Simpson (1980) and our own experimental data. The line describing the similarity phase intersects the constant-velocity line at approximately 10 lock lengths, as expected from the results of the standard lock release on an impermeable base. Also included in figure 7(*b*) is the evolution given by the integral model over a porous bottom (2.32)–(2.33) and a solid bottom ($M = 1$ in (2.33)). As seen, the integral model is only a fair approximation for the evolution of the front position itself with and without loss of mass. However, it should be recalled that the model provides the rough correction M_1 needed for calculating the evolution of the current mass over the porous medium with the integral model (2.20).

Figure 7(*c*) shows that the speeds developed by the currents initially are slightly slower than those provided by the energy conserving solution of Benjamin (1968) with the same boundary conditions at the top and the bottom of the channel, for which $F_0 = 0.5$. However, the value $F_0 = 0.46 \pm 0.02$ obtained here is within the experimental error of the Froude number for lock-release experiments performed with an impermeable base and an upper free surface (Rottman & Simpson 1983; Shin *et al.* 2003). This suggests that the initial value of u_f for $t/t_0 \lesssim 15$ is not strongly modified by the presence of the porous medium for any value of λ under the present experimental conditions. The initial velocity of the front is then determined by h_0 and g_0', as expected for the lock-exchange problem.

Subsequently, the front tends asymptotically to the self-similar solution for gravity currents running over a solid bottom as indicated by the dashed line in figures 7(*b*) and (*c*). We also see that there is no appreciable difference between the evolution of the fronts in our experiments and the solid bottom case, suggesting that the reduction of the global mass has not influenced the leading part of the current at this time in its motion. However, for the latest times of the evolution that difference increases as shown in figure 7(*c*), and the evolution of the experimental points seems to follow the trend indicated by the solution of the integral model with the permeable base (dash-dotted line).

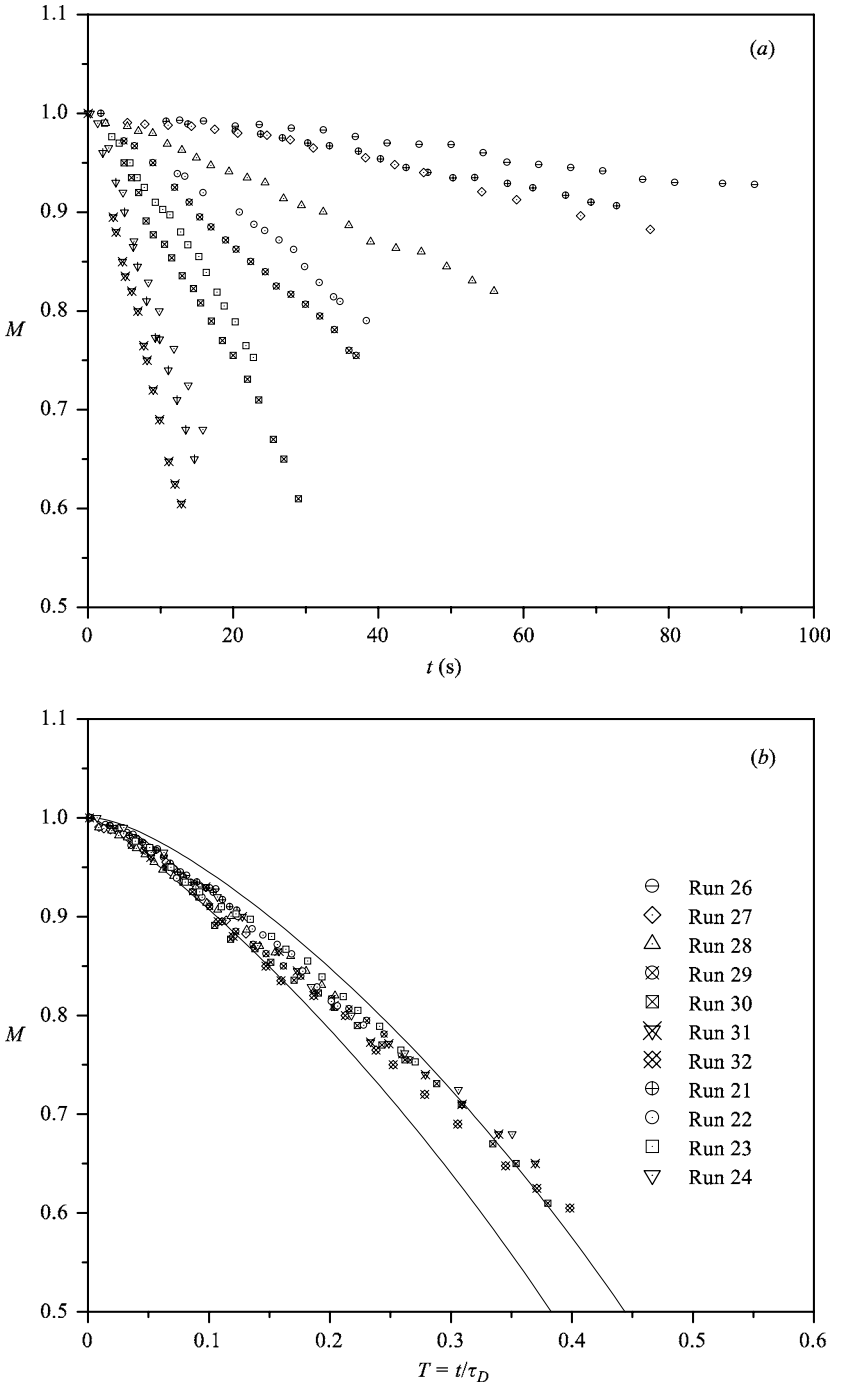

FIGURE 6. Dimensionless mass M remaining in the current for a porous bed of thickness $D = 9$ cm with different a_0 and g'_o as a function of (a) time t measured from release, and (b) dimensionless time formed by using (2.13). The solid lines correspond to the solutions of the integral model with minimum (60) and maximum (600) values of λ of the experiments.

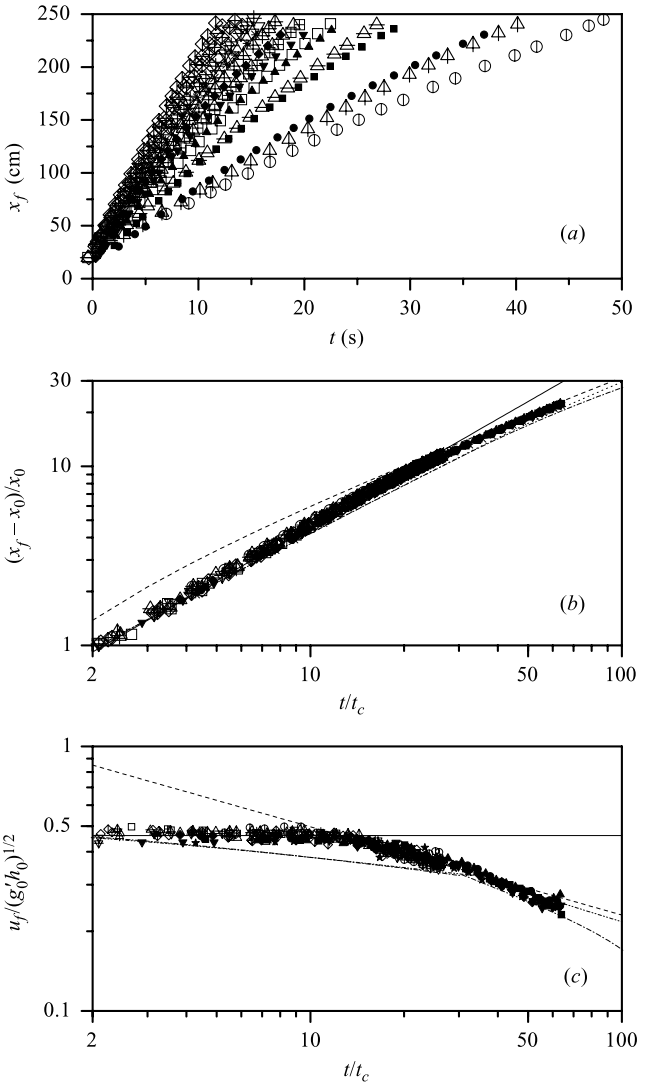

FIGURE 7. Evolution of the front position (a, b) and the front velocity (c) of the gravity currents for $D = 12\,\text{cm}$. The experiments 1-6, with $a_0 \approx 250\,\text{cm}^2$ are shown by solid symbols, while the runs 7-20 ($a_0 \approx 500\,\text{cm}^2$) by open symbols. The solid and dashed lines correspond to the theoretical evolution in the constant-velocity phase and the self-similar phase for impermeable bases, respectively. The dash-dotted and dash-dot-dot lines correspond to the solution of the integral model with and without mass losses, respectively.

Figures 5(b) and 6(b) show a systematic deviation of the last points in the experiments with higher g_0' that might indicate the presence of another flow regime. Reynolds numbers Re_c of the currents, where

$$Re_c = \frac{h_f}{\nu}\frac{\mathrm{d}x_f}{\mathrm{d}t}$$

and h_f the height of the current at the front, were measured to be high ($Re_c > 4000$) even in the later stages of the experiments. Further, there is no evidence of a transition to the $x \propto t^{1/5}$ expected for the viscous regime in figure 7. We believe these deviations

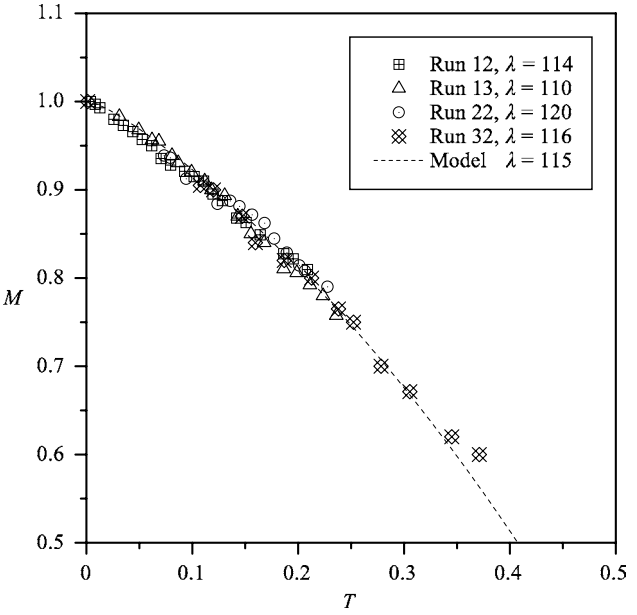

FIGURE 8. Comparison of the dimensionless mass $M(T)$ in four cases that have similar λ coming from different combinations of a_0, D and g'_o. The dashed line is the corresponding solution provided by the integral model.

are a result of residual error in the definition of the level of the porous medium and the refraction index correction applied in the image processing described in § 3, because they appear for the smallest heights and the densest gravity currents where the error in the measurements is largest.

According to (2.32)–(2.33), the theoretical curve for $M(T)$ is unique for a given λ, regardless of the individual values of a_0, g'_0 and D. As shown in figure 8, this behaviour is also found when comparing the time evolution of M obtained in experiments with analogous values of λ.

From comparisons between theoretical and experimental evolution of $M(T)$ such as those shown in figure 7, we determined, for each experiment, the value λ_{expt} that minimized the mean square deviation between the theoretical curve and the experimental values of $M(T)$. Accordingly, we obtain $\tau_{\text{expt}} = \lambda_{\text{expt}} \times t_c$ that can be compared directly with τ_D given by (2.13). Figure 9 shows the resulting τ_{expt} as a function of g'_0/D for all the experiments. It is seen that there is no dependence of $a_0 = x_0 h_0$ as expected from the theoretical relationship (2.13). The best fit line of the experimental points $\tau_{\text{expt}} = C(D/g'_0)$ is also shown in the figure. Comparison with (2.13) shows that $C = \nu/k$, and, therefore, the coefficient of the best fit line allows us to obtain the permeability k of the porous material. Using $\nu = 1.1 \times 10^{-6}\ \text{m}^2\ \text{s}^{-1}$, we obtain $k \simeq 6 \times 10^{-5}\ \text{cm}^2$. This value agrees well with that estimated using the Kozeny–Karman equation ($k = 6.14 \times 10^{-5}\ \text{cm}^2$) (see Duillen 1979 or Fand *et al.* 1987).

In addition, knowledge of the evolution of the mass remaining in the current makes possible to calculate the Reynolds number $Re_\eta = \overline{w_\eta}\, d/\nu$ of the flow through the porous medium, where $\overline{w_\eta}$ is obtained from (2.12) and d is the diameter of the glass spheres. It is found that $Re_\eta < 5$ in all experiments and, in most of the runs $Re_\eta < 1$. These values, and the estimate of the permeability described above, supports the use of Darcy's law for the flow within the porous medium (Fand *et al.* 1987).

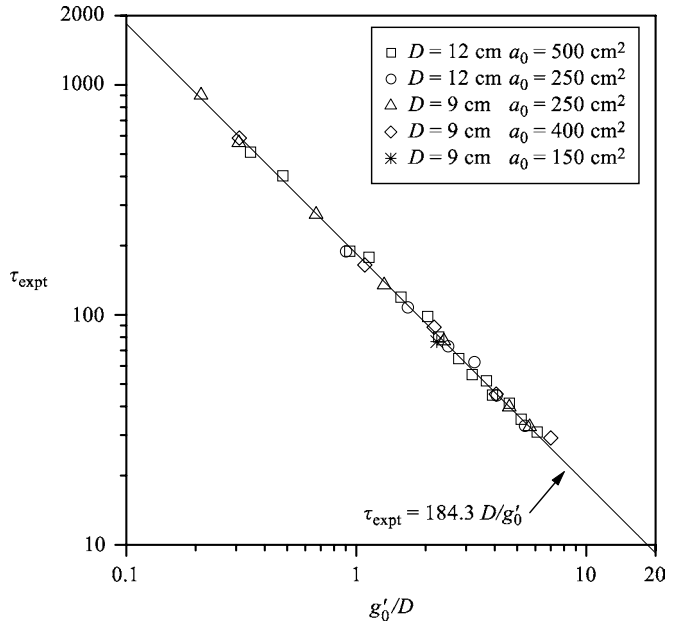

FIGURE 9. Experimental measurements of τ_{expt} as function of g_c'/D. As suggested by the time scale given by (2.13), results coming from experiments performed with different a_0 introduce no deviations from the general trend.

5. Summary and conclusions

Plane inertial gravity currents travelling over a thick porous bed consisting of small glass spheres were investigated. This work is an extension of previous experiments by Thomas *et al.* (1998), where the porous bed was represented by a thin grid. The currents were produced by lock-release of salt water in a channel containing fresh water. The porous bed was initially saturated with fresh water, which was displaced by the dense fluid in the current as it moved over the bed.

The progress of the front position of the currents was measured directly and the corresponding velocity was calculated. From the measurements of the fluid mass lost from the current, we are able to estimate the flow of these fluid through the bed to confirm that it is well described by Darcy's law and scales on a time scale $\tau_D = \nu D/kg_0'$. This time scale was also found by Thomas *et al.* (1998) for the flow of fluid coming from a gravity current running over a permeable base made from a thin mesh, despite the fact that subsequent experiments performed by Marino & Thomas (2002) indicated that Darcy's law is not valid at all times.

We present results of a model that describes the flow of the current in terms of a local Froude number at the front, and a global mass balance suggesting an analytical approximation, (2.20), for extended currents over thick porous layers: the mass evolution does not depend on the height profile, mixing, Froude number at the front, details of the beginning of the flow including the evolution of the bore, and the initial fractional depth of the dense fluid. For a better comparison between the loss of fluid from the current and the laboratory results, we introduce a simple correction through an integral model obtaining (2.32)–(2.33) with proper initial conditions and F function, and achieving a good agreement. In addition, the current may decelerate as the driving pressure is reduced because of the current thinning due to the sinking

of fluid into the bed, but significant changes in the evolution of the front position or its velocity take place outside the maximum extension of the present experiments.

The findings reported cover the full-depth release case. However, some preliminary experiments performed for partial-depth release shown no significant difference of the behaviour of the gravity currents during the initial stages with respect to those described by Huppert & Simpson (1980), or at the later times with respect to those introduced here.

Thus the present experimental work and analysis extend our previous work over thin permeable surfaces to gravity currents on thick porous beds. The experiments are arranged so that the fresh water within the bed can be displaced downwards and out through the bottom of the bed. In other practical cases this may not be possible and the only exchange will occur by the gravitational driven flow within the bed. We observed this flow, but in our present arrangement it was of secondary importance. Further work is needed to investigate this case.

L. P. T. and B. M. M. acknowledge financial support from CONICET and UNCPBA, Argentina.

REFERENCES

Acton, J. M., Huppert, H. E. & Worster, M. G. 2001 Two-dimensional viscous gravity currents flowing over a porous medium. *J. Fluid Mech.* **440**, 359–380.

Bear, J. 1972 *Dynamics of Fluids in Porous Media.* Elsevier.

Benjamin, T. B. 1968 Gravity currents and related phenomena. *J. Fluid Mech.* **31**, 209–248.

Dalziel, S. B. 1995 *DigImage: System Overview*. Cambridge Environmental Research Consultants, UK.

Darcy, H. P. G. 1856 *Les Fontaines Publiques de la Ville de Dijon.* Paris.

Didden, N. & Maxworthy, T. 1982 The viscous spreading of plane and axisymmetric gravity currents. *J. Fluid Mech.* **121**, 27–42.

Duillen, F. A. L. 1979 *Porous Media. Fluid Transport and Pore Structure*. Academic, New York.

Fand, R. M., Kim, B. Y. K., Lam, A. C. C. & Phan, R. T. 1987 Resistance to the flow of fluids through simple and complex porous media whose matrices are composed of randomly packed spheres. *J. Fluids Engng* **109**, 268–274.

Fannelop, T. K. & Waldman, W. 1972 Dynamics of oils slicks. *AIAA J.* **10**, 506–510.

Fay 1969 The spread of oils slicks on a calm sea. In *Oil on the Sea* (ed. D. P. Hoult), pp. 43–63. Plenum.

Hacker, J., Linden, P. F. & Dalziel, S. B. 1996 Mixing in lock-release gravity currents. *Dyn. Atmos. Oceans* **24**, 183–195.

Hoult, D. P. 1972 Oil spreading on the sea. *Annu. Rev. Fluid Mech.* **4**, 341–368.

Huppert, H. E. 1982 The propagation of two-dimensional and axisymmetric viscous gravity currents over a rigid horizontal surface. *J. Fluid Mech.* **121**, 43–58.

Huppert, H. E. & Simpson, J. E. 1980 The slumping of gravity currents. *J. Fluid Mech.* **99**, 785–799.

Linden, P. F. & Simpson, J. E. 1986 Gravity driven flows in a turbulent fluid. *J. Fluid Mech.* **172**, 481–497.

Marino, B. M., Thomas, L. P., Diez, J. A. & Gratton, R. 1996 Capillary effects on viscous gravity spreading of wetting liquids. *J. Colloid Interface Sci.* **177**, 14–30.

Marino, B. M. & Thomas, L. P. 2002 The spreading of a gravity current over a permeable surface. *J. Hydraulic Engng* **128**, 1–7.

Merzkirch, W. 1987 *Flow Visualisation.* Academic Press.

Moodie, T. B. & Pascal, J. P. 1999*a* Downslope movement of compositionally driven gravity currents over porous surfaces. *J. Porous Media* **2**, 127–141.

Moodie, T. B. & Pascal, J. P. 1999*b* Axisymmetric spreading and filtration of inclined thermals over porpous surfaces. *Can. Appl. Math. Q.* **7**, 185–201.

Rottman, J. W. & Linden, P. F. 2001 Gravity currents. Chap. 4, In *Stratified Flows in the Environment* (ed. R. H. J. Grimshaw), Kluwer.

Rottman, J. W. & Simpson, J. E. 1983 Gravity currents produced by instantaneous releases of a heavy fluid in a rectangular channel. *J. Fluid Mech.* **135**, 95–110.

Shin, J. O., Dalziel, S. B. & Linden, P. F. 2002 Gravity currents produced by lock exchange. *J. Fluid Mech.* (submitted).

Simpson, J. E. 1997 *Gravity Currents: In the Environment and the Laboratory*. Cambridge University Press.

Thomas, L. P., Marino, B. M. & Linden, P. F. 1998 Gravity currents over porous substrates. *J. Fluid Mech.* **366**, 239–258.

Ungarish, M. & Huppert, H. E. 2000 High–Reynolds–number gravity currents over a porous boundary: shallow–water solutions and box–model approximations. *J. Fluid Mech.* **418**, 1–23.